IOSR Journal of Applied Chemistry (IOSR-JAC)
e-ISSN: 2278-5736.Volume 12, Issue 2 Ser. I (February. 2019), PP 65-80
www.iosrjournals.org

Simultaneous Detection of Anthracene and Phenanthrene on Ag-Au alloy nanoparticles/overoxidized-polypyrrole Composite Modified Carbon Electrode

Stephen Nzioki Mailu
Department of Physical Sciences, Machakos University, P.O. Box 136-90100, Machakos, Kenya.
Corresponding Author: Stephen Nzioki Mailu

Abstract: *A simple and highly selective amperometric sensor for simultaneous determination of anthracene (AN) and phenanthrene (PHE) has been developed based on a composite of overoxidized-polypyrrole (PPyox) and Ag-Au alloy nanoparticles (Ag-AuNPs). UV-visible confirmed the formation of the Ag-Au alloy nanoparticles and transmission electron microscopy (TEM) revealed a rather uniform distribution of several nanometer-sized particles (20-30 nm). Voltammetric interrogations using ferricyanide redox probe showed that the composite (PPyox/Ag-AuNPs) had a higher catalytic effect compared to Ag-AuNPs and PPyox films. The sensor (PPyox/Ag-AuNPs composite-coated GCE) was interrogated with cyclic voltammetry (CV) and square wave voltammetry (SWV) in acetonitrile containing 0.1 M $LiClO_4$. The sensing surface with the Ag-Au ratio of 1:3 was able to oxidize AN and PHE at different potentials when operated in the presence of both analytes. A successful elimination of the fouling effect by the oxidized products of AN and PHE was achieved at the modified electrode. The catalytic peak currents obtained from SWV increased linearly with increasing AN and PHE concentrations in the range of 30 μM to 312 μM and 30 μM to280 μM with a detection limit of 23.05 μM and 24.406 μM, respectively.*

***Keywords*:** *Anthracene, Phenanthrene, Polyaromatic hydrocarbons, Overoxidized-polypyrrole, Composite.*

Date of Submission: 04-02-2019 Date of acceptance:22-02-2019

I. Introduction

Bimetallic nanoparticles such as alloy and core-shell particles are of considerable interest in various fields of science and engineering because of their composition and size-dependent electrical, chemical, optical and catalytic properties [1]. They are of special importance in the field of catalysis as they exhibit better catalytic properties than their monometallic counterparts [2]. Depending on the synthesis method, the resulting bimetallic particles can exhibit alloy behavior or core-shell system behavior. The alloy nanoparticles are homogeneously distributed over the whole volume on an atomic scale while the core-shell nanoparticles constitute the core of the structure, and the other one the external shell [2]. Bimetallic nanoparticles can be prepared by simultaneous reduction or by successive reduction of the two metal ions in the presence of suitable stabilization strategy such as steric hindrance and static-electronic repulsive force. The former reduction method leads to the formation of a particle structure of homogeneous alloy, while the latter to the production of core–shell structure particles [2]. The structures of bimetallic combinations depend on the preparation conditions, miscibility and kinetics of reduction of the metal ions [3]. Gold is very useful as an alloying metal due to its relatively low reactivity and has been used in conjunction with metals such as palladium and platinum for various catalytic reactions [3]. For example, combinations such as Au-Pd and Au-Pt are reported to exhibit a core-shell type of structure, while Au-Ag forms homogenous alloys when reduced simultaneously. Au and Ag have very similar lattice constants and are completely miscible over the entire composition range which leads to the formation of highly catalytic single-phase alloys of any desired composition of Au and Ag [3]. It has been reported that Ag-Au alloy nanoparticles have excellent electrocatalytic properties. According to Masato *et al*., [4] electrochemical properties and the electrocatalytic properties of Ag-Au alloy nanoparticles with different Ag and Au composition depends on the amount of Ag in the bimetallic alloy nanoparticles. However, Aiqin Wang *et al*. and Xhiang *et al*. showed that Ag-Au bimetallic alloy nanoparticles portrayed better electrocatalytic properties when Ag:Au was in the ratio of 1:3 [5,6].

On the other hand, polypyrrole (PPy) is a conducting polymer which is an excellent material used as a matrix for deposition of metal nanoparticles [7]. PPy film has excellent properties for its application such as the ease of its monomer pyrrole to be oxidized, water soluble, commercially available and the PPy posses good environmental stability, good redox properties, high electrical conductivity, simplicity of synthetic procedures and the possibility of forming homopolymers or composites with optical, chemical and physical properties [8].

The PPy film can further be overoxidized at high potential and lose its conductivity [7]. It has been reported that during overoxidation process, the doping ions are expelled from the polymer film, and oxygen-containing groups such as carbonyl and carboxyl groups are introduced to the pyrrole unit. This transformation of PPy as a result of overoxidation is accomplished by a loss of conjugation, electronic conductivity and dedoping with a net electronegative character imparted to the polymer film [7]. The overoxidation of polypyrrole where the dopant (A^-) is ClO_4^- may be represented by the simplified process shown in scheme 1.

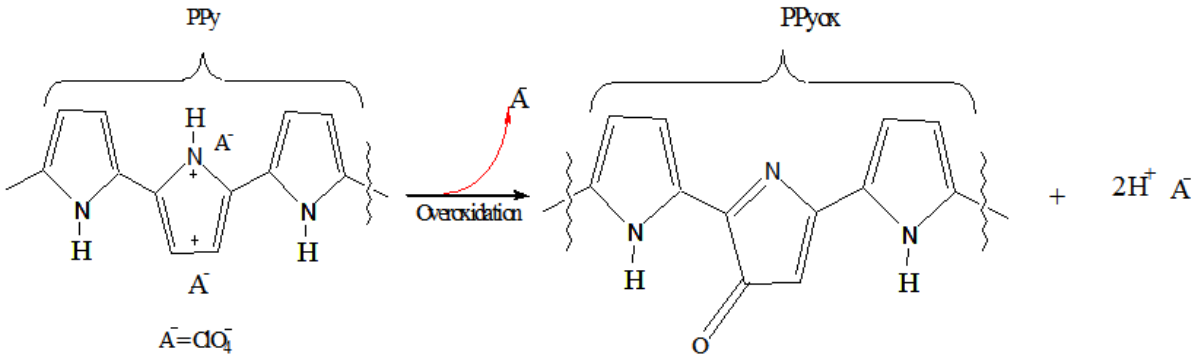

Polypyrrole (doped) Overoxidized polypyrrole (dedoped)

Scheme 1: A scheme showing the overoxidation process of polypyrrole.

The small doping anions (ClO_4^-) ejected from the PPyox film, creates a porous structure on the electrode which creates room for the deposition of the nanoparticles [7]. The PPy film improves selectivity, cation permselective behavior and the efficiency of PPyox in suppressing interfering electroactive species and avoiding electrode fouling [7]. The high permselectivity of overoxidized polypyrrole films allows analytes to reach the surface of electrodes easily.

The overoxidized PPy film has excellent cation exchange and molecular sieve properties. Several applications of PPyox film has been reported in literature. For example, PPyox film has been used in the fabrication of H_2O_2, glucose and cholesterol biosensors [7]. Due to permselective behavior of the film, the sensors provided an efficient barrier to exclude interferents and protect the electrode from fouling. PPyox film has also been used in the detection of isoniazid in pharmaceuticals, as a porous template for DNA immobilization for the detection of dopamine and serotonin [7]. However, much work has not been done on the deposition of metal nanoparticles on the porous PPyox film. Li *et al*. [7] reported the deposition of gold nanoparticles on the PPyox film and the composite was used as a sensor for the simultaneous detection of epinephrine and uric acid in the presence of ascorbic acid. To our best knowledge, the use of alloy nanoparticles deposited on PPyox film has never been reported.

Polycyclic aromatic hydrocarbons (PAHs) are organic contaminants of great environmental concern and are known to be teratogenic, carcinogenic and mutagenic [9]. They are ubiquitous pollutants and are always found as a mixture of individual compounds [10-11]. PAHs are mainly formed during incomplete combustion processes and enter the environment via the atmosphere. Their origin can be found in oil and coal consuming industrial processes, fires, traffic, heating as well as cooking and tobacco smoking. They can be found airborne, in the gas phase or adsorbed to airborne particles, in aqueous phases, such as groundwater, waste water or drinking water, and adsorbed to solids in soil or sediment [12]. The carcinogenic and mutagenic potential of some of the PAHs and their ubiquity in the environment led to the inclusion of 16 PAHs compounds in the list of priority pollutants in waste water published by the United States (US) Environmental Protection Agency (EPA) 1984 [13-15] and later adopted by the US government in 1988. As a result of their carcinogenic and toxicological effects, several methods have been applied in their determination such as immunoassay [16], gas chromatography [17] and high performance liquid chromatography (HPLC) with UV-vis absorbance or fluorescence [18-19] and capillary electrophoresis (CE) equipped with laser-induced fluorescence [20]. The drawbacks of these methods although the most accurate, are that they are expensive, time consuming, require large sample volumes as well as large amount of organic solvent with separation and extraction procedures, and must be undertaken by an analytical chemist in a dedicated analytical laboratory [21]. Moreover, the low solubility of the highly hydrophobic hydrocarbons in water and their occurrence in complex mixtures often require complex extraction, preconcentration and separation procedures for the sensitive detection of the PAHs.

Most immunoassays for PAHs described in literature are enzyme linked immunosorbent assays (ELISA) [22-24], although other techniques such as radioimmunoassay (RIA) [25-26], piezoelectric immunosensor [27], capacitive immunosensor [28] and fluorescence based fiber optical immunosensors [29],

have also been investigated. However, the fact that many PAHs are very similar in molecular structure, electron density and molecular weight and the lack of side groups makes it impossible to produce antibodies specific for only one compound [30]. This poses a challenge in the application of immunoassays for determination of PAHs. These limitations can be reduced or avoided by using biosensor systems. Several biosensors including immunosensors, DNA biosensors and whole-cell biosensors have been developed for the determination of PAHs [30-34]. For example, a disposable amperometric immunosensor using screen-printed electrode was fabricated to detect low concentration of Phenanthrene [30]. A soil biosensor using a recombinant biolumiscent bacterium, Escherichia coli GC2, and rhamnolipids, a biosurfactant to increase the bioavailability of PAHs from the contaminated soil has been developed [31-34]. In addition, a flow injection analysis system coupled with an evanescent wave biosensor for the detection of aromatic compounds that can intercalate with dsDNA has also been reported [33]. However, these biosensors are designed for the determination of a single analyte in a sample at a time and lack the opportunity for the high-thorough analysis of multiple samples in the presence of multianalytes [35]. Consequently, the need for simultaneous determination of phenanthrene (PHE) and anthracene (AN) as some of the identified priority PAHs pollutants by the United States Environmental Protection Agency (USEPA) [36] is of great importance due to their similar structures, properties and their acute toxicity. There is an ever-increasing demand for the determination of trace amounts of these substances at plant sites, water bodies and air. This demand for the development of a suitable and cost-effective analytical method to carry out a rapid, simple and sensitive analysis of these PAHs in environmental samples. Electroanalytical methods are considered to be better methods for the determination of PAHs and an efficient solution to environmental problems compared to the other methods because a completely clean reagent, i.e. the electron, is utilized [30, 37]. However, during the determination of the PAHs using the electroanalytical methods, electrode fouling is observed which affects the stability of the methods. It is thus of great importance to develop an electrochemical method that is free from electrode fouling, highly sensitive, simple, less time consuming and that is able to determine more than one PAH in a sample.

This study entailed the deposition of Ag-Au alloy nanoparticles on insulating PPyox film modified glassy carbon electrode (PPyox/Ag-AuNPs/GCE) to develop a novel electrochemical sensor for simultaneous detection of AN and PHE. The PPyox/Ag-AuNPs/GCE not only exhibited strong catalytic activity towards the oxidation of AN and PHE, but also showed strong antifouling properties.

II. Experimental Methods

2.1 Reagents and Materials

Analytical grade pyrrole (Py) (99%), hydrogen tetrachloroaurate(III) trihydrate ($HAuCl_4.3H_2O$), trisodium citrate ($Na_3C_6H_5O_7$) (99%), silver nitrate ($AgNO_3$) (99%), anthracene (99%), phenanthrene (99%), lithium perchlorate ($LiClO_4$) (99.99%), acetonitrile (HPLC grade) were obtained from Sigma-Aldrich. All chemicals were used as received except pyrrole which was double distilled under nitrogen before use. Ultra pure water (Millipore) was used for all preparations. Anthracene and phenanthrene working solutions were prepared in acetonitrile.

2.2 Measurement and Instrumentation

Voltammetric measurements were performed on a BAS 50B electrochemical analyzer from Bioanalytical systems inc. (West Lafayette, IN) with conventional three- electrode system consisting of glassy carbon electrode (GCE), Ag/AgCl (saturated NaCl) and platinum wire as working, reference and counter electrodes, respectively. Lithium perchlorate was used as the supporting electrolyte. All experimental solutions were purged with high purity argon gas and blanketed with argon atmosphere during measurements. The experiments were carried out at controlled room temperature (25 °C). UV-Vis spectra measurements were recorded on a Nicolette Evolution 100 Spectrometer (Thermo Electron Corporation, UK). Transmission electron microscopy (TEM) images were acquired using a Tecnai G^2 F_2O X-Twin MAT. TEM characterizations were performed by placing a drop of the solution on a carbon coated copper grid and dried under electric bulb for 30 min. Electrochemical impedance spectroscopy (EIS) measurements were recorded with Zahner IM6ex Germany, at perturbation amplitude of 10 mV within the frequency range of 100 kHz–100 mHz.

2.3 Preparation of Silver-Gold Alloy Nanoparticles (Ag-AuNPs)

Silver-gold alloy nanoparticles (Ag-AuNPs) were synthesized through chemical methods [38-39]. 49 mL of water was added into a 100 mL round bottomed flask. 0.5 mL 2% (w/v) sodium citrate was added into the water and the reaction mixture heated to 92 °C. 0.5 mL of a mixture of 10 mM $HAuCl_4$ and 10 mM $AgNO_3$ solution was added into the reaction mixture and the temperature regulated between 90 °C and 92 °C and refluxed for 1 hour. The volume of the mixture was adjusted so as to prepare Ag-Au with Ag:Au ratio of 1:3 by mixing 0.125 mL of 10 mM $AgNO_3$ and 0.375 mL 10 mM $HAuCl_4$. There was a colour change observed in the solution (dark red) indicating the formation of nanoparticles according to the hallmarks reported in the in the

literature [40]. For control purposes, silver nanoparticles (AgNPs) and gold nanoparticles (AuNPs) were, respectively, prepared by the same method [41-42]. For electrochemical characterization of the nanoparticles, 4 µL solutions of already synthesized Ag-Au alloy nanoparticles were drop-coated on glassy carbon electrode (GCE) and denoted as Ag-AuNPs/GCE.

2.4 Fabrication of Over-Oxidized Polypyrrole/Ag-AuNPs Composite Film-Modified Electrode (PPyox/Ag-AuNPs/GCE)

Prior to modification, the bare GCE was polished to a mirror finish using 1.0, 0.3, and 0.05 µm alumina and sonicated successively in ethanol and water. Electrochemical polymerization of pyrrole was carried out in 0.1 M $LiClO_4$ solution containing 0.1 M pyrrole by cycling the potential from -400 to 700 mV at a scan rate of 50 mV s^{-1} for 10 cycles. The electrode was rinsed with water and then transferred into 0.1 M NaOH solution for electrochemical overoxidation of the conductive PPy film at + 1.0 V for 7 min. The resulting modified electrode was ready for use after rinsing with water and henceforth denoted as PPyox/GCE. In order to incorporate the intermetallic nanoparticles, 4 µL solution of already synthesized Ag-Au alloy nanoparticles were drop-coated on the PPyox/GCE and allowed to dry at room temperature. The modified electrode was taken out and rinsed with water, and henceforth denoted as PPyox/Ag-AuNPs/GCE.

III. Results and Discussion

3.1 Characterization of Silver-Gold Alloy Nanoparticles (Ag-AuNPs)

Ag-Au alloy nanoparticles were obtained through the simultaneous reduction of silver and gold ions using sodium citrate [38]. This was confirmed by optical spectroscopy. If pure silver and gold nanoparticles are mixed physically in the same solution, two absorption peaks are expected to be observed, whereas for alloys, a single absorption peak is expected (Angshuman *et al*., 2008). Appearance of a single absorption peak in Fig. 1 (A) for colloidal solution of Ag-Au (1:3) alloy nanoparticles (curve b), confirmed the formation of alloy nanoparticles. From Fig. 1 (A), it is observed that for Ag and Au nanoparticles, the absorption peaks appeared at 415 and 525 nm, respectively. For the alloy nanoparticles, the absorption peak appeared at 504 nm [39, 43]. The appearance of a single absorption peak indicates that synthesized Ag-Au bimetallic particles are in alloy form rather than being a mixture of individual nanoparticles, whereas the physical mixture of the synthesized Ag and Au nanoparticles showed two absorption peaks corresponding to the individual metal nanoparticles (Fig. 1 (A), curve d). This is a confirmation that the synthesized nanoparticles were alloys and not mixture of elemental nanoparticles [44]. Fig. 1 (B) gives the comparative data at zero storage time (immediately after synthesis of the nanoparticles), represented by lower letter case letters (a-c), and data after 4 months' storage at 25 °C (room temperature) represented by capital letters (A-C). Not much shift in absorption peaks was observed after 4 months' storage, indicating the formation of highly stable alloy nanoparticles. The alloy formation can be attributed to similar lattice constants of 0.408 and 0.409 nm, for gold and silver, respectively. This small difference in lattice constants, being smaller than the amplitude of thermal vibrations of atoms, has already been hypothesized to favor alloy formation even at the nanometer scale [45].

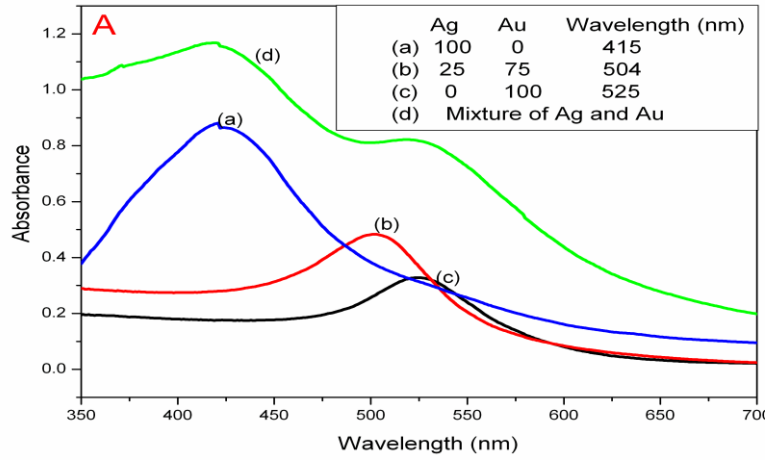

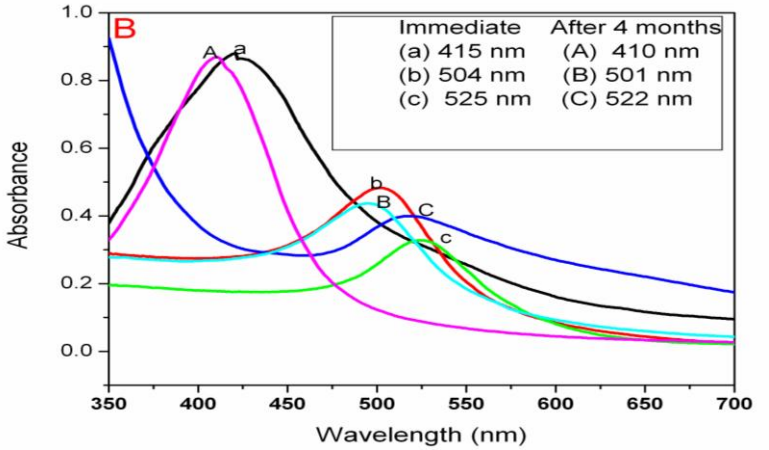

Figure 1. (A) UV-visible absorption spectra of Ag (curve **a**), Au (curve **c**), Ag-Au alloy (1:3) (curve **b**) nanoparticles and a mixture of pure Ag and Au nanoparticles (curve **d**). **(B)** UV-visible absorption spectra of Ag, Ag-Au alloy and Au nanoparticles at different storage times (immediately after synthesis and after 4 months' storage).

The size and shape of the nanoparticles were determined using transmission electron microscopy (TEM). From Fig. 2 (a), particle sizes in the range of 20-30 nm was observed for Ag-Au (1:3) alloy nanoparticles. There was no agglomeration of the nanoparticles observed from the TEM image. The optical properties of the nanoparticles differ depending on the type (kind) of the nanoparticles as can be seen from the digital photographs in Fig. 2 (b).

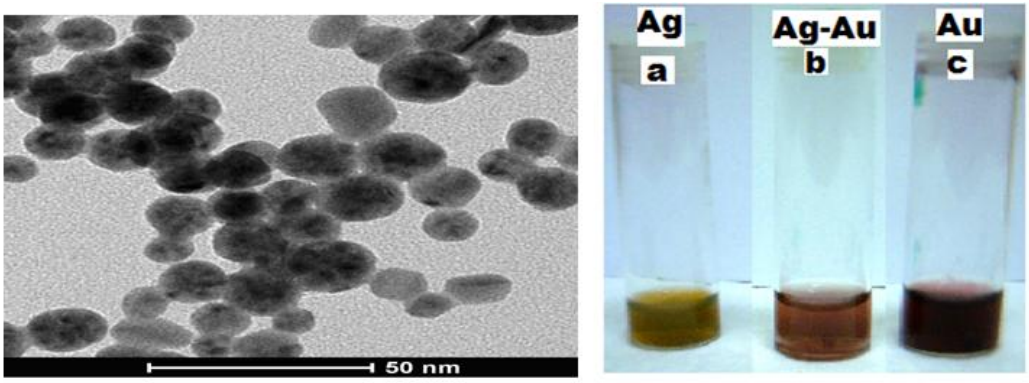

(a) **(b)**

Figure 2. **(a)** TEM image of Ag-Au (1:3) bimetallic alloy nanoparticles. **(b)** Digital photographs of Ag, Ag-Au (1:3) alloy and Au nanoparticles.

3.2 Electrochemical Characteristics of Ag-AuNPs/GCE in $LiClO_4$ and $[Fe(CN)_6]^{3-/4-}$

The preparation process of electrodes was monitored by electrochemical impedance spectroscopy (EIS) in 0.1 M $LiClO_4$ as well as KCl (0.1 M) solutions containing $[Fe(CN)_6]^{3-/4-}$ and plotted in the form of complex plane diagrams (Nyquist plots) and bode plots with a frequency range of 100 kHz to 0.1 Hz. The amplitude of the applied sine wave potential was 10 mV, whereas the ambient applied dc potential was set at the formal potentials which were obtained from a CV experiments of the $[Fe(CN)_6]^{3-/4-}$ redox probe.

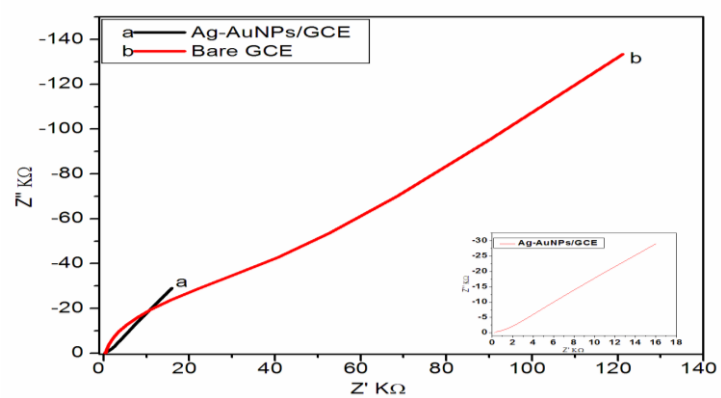

Figure 3a. Nyquist plot of Ag-AuNPs/GCE (curve **a**) and bare GCE (curve **b**) at a potential of -400 mV in 0.1 M $LiClO_4$.

At -400 mV, the R_{ct} of the Ag-AuNPs modified electrode was much smaller with a value of 4164 Ω as compared to 42670 Ω obtained for the bare GCE as shown in Fig. 3a which revealed that the nanoparticles facilitated the flow of ions. The increase in conductivity of the alloy nanoparticles may be attributed to small size of the nanoparticles which increases the surface area of the conducting surface of the electrode.

Besides the impedance modulus change, we observed a change in the phase angle after GCE was modified with the alloy nanoparticles. Fig. 3b shows the plot of phase angle versus frequency for the bare GCE and modified electrode. The bode plot showed a remarkable difference in the electrochemistry of the bare and the modified electrode. Phase angle shift was observed for bare electrode (18.6°) at high frequency region to lower frequency with decrease in impedance modulus due to modification with Ag-Au alloy nanoparticles (3.4°). The EIS spectra also showed that at low frequency (100 mV) when the electronic of the electrode system was minimally perturbed, the Ag-AuNPs/GCE exhibited greater semiconductor behaviour (higher phase angle value of 61.1°) than the bare GCE (47.8°). Consequently, an improved conductivity of the modified electrode over bare GCE can be observed by the marked reduction in the impedance.

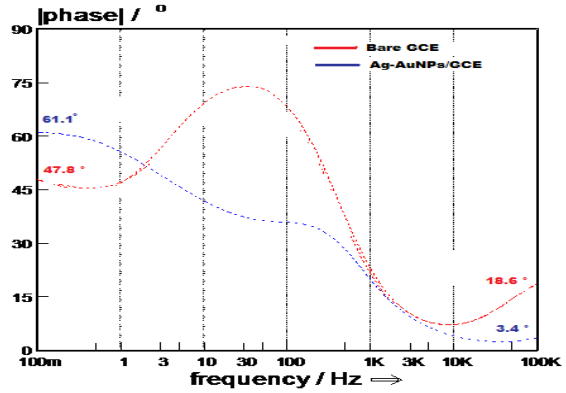

Figure 3b. Bode-phase plots of bare GCE (red) and Ag-AuNPs/GCE (blue) at a potential of -400 mV in 0.1 M $LiClO_4$.

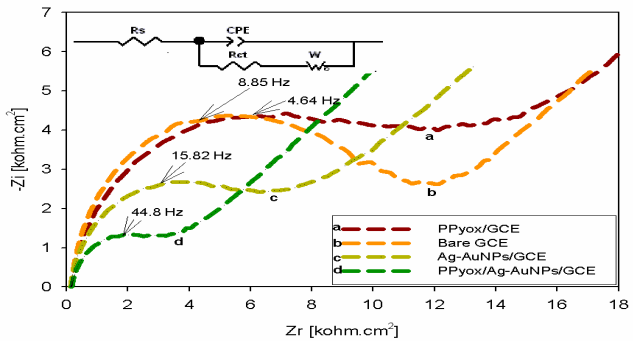

Figure 4. Nyquist plots of the EIS recorded in the presence of the $K_4[Fe(CN)_6]/K_3[Fe(CN)_6]$ (1:1) containing aq. KCl (0.1 M) for the PPyox/GCE (curve **a**), bare GCE (curve **b**), Ag-AuNPs/GCE (curve **c**) and PPyox/Ag-AuNPs/GCE (curve **d**).

From Fig. 4, significant difference of R_{ct} was observed upon the formation of the modified electrode as compared to the bare GCE. The R_{ct} value for the bare GCE (curve b) was 9.125×10^3 Ω. After the PPyox film was deposited on the GCE, the R_{ct} value was found to be 9.684×10^3 Ω (curve a). As compared to the bare GCE, the R_{ct} of PPyox/GCE increased. This can be attributed to the negatively charged and the low conductive PPyox film. The negative charge of the layer should be unfavorable for the approaching of ferricyanide anions. After the bare GCE was modified with Ag-AuNPs, the R_{ct} value (4.674×10^3 Ω) decreased obviously (curve c) implying that the Ag-AuNPs played an important role in accelerating the transfer of electrons. For the PPyox/Ag-AuNPs/GCE, the R_{ct} value (2.800×10^3 Ω) decreased further (curve d) an indicator that the composite was more facile to the electron transfer.

From ω_{max} (frequency at maximum imaginary impedance of the semicircle), useful kinetic parameters of $Fe(CN)_6^{4-} \leftrightharpoons Fe(CN)_6^{3-} + e^-$ electron transfer such as time constant (cycle life) τ, exchange current I_0, and heterogeneous rate constant k_{et} [46-47] were calculated from equations (1, 2, 3, and 4) and shown in table 1.

$$\omega_{max} = \frac{1}{R_{ct}C_{dl}} \quad (1)$$

$$\tau = R_{ct}C_{dl} \quad (2)$$

$$I_0 = \frac{RT}{nFR_{ct}} \quad (3)$$

$$K_{et} = \frac{I_0}{nFAC_0} \quad (4)$$

Where $\omega_{max} = 2\pi f$, C_{dl} is the double layer capacitance, R = 8.314 J K^{-1} mol^{-1}, F = 96 486 C mol^{-1}, n =1, C_0 is the concentration of $[Fe(CN)_6]^{3-/4-}$ = 5 x 10^{-6} mol cm^{-3}. The maximum frequency values (f) where taken from Fig. 4.

Table 1. Effect of PPyox/Ag-AuNPs electrode on the kinetics of $[Fe(CN)_6]^{3-/4-}$

Kinetic parameters	PPyox/GCE	Bare GCE	Ag-AuNPs/GCE	PPyox/Ag-AuNPs/GCE
ω_{max} (rad s^{-1})	29.160	55.610	99.430	281.520
τ (s rad^{-1})	3.429 x 10^{-2}	1.798 x 10^{-2}	1.005 x 10^{-2}	3.552 x 10^{-3}
I_0 (A)	2.652 x 10^{-6}	2.814 x 10^{-6}	5.493 x 10^{-6}	9.171 x 10^{-6}
k_{et} (cm s^{-1})	7.740 x 10^{-5}	8.215 x 10^{-5}	1.604x10^{-4}	2.677 x 10^{-4}

AuNPs/GCE are 2.652 x 10^{-6} A and 9.171 x 10^{-6} A, respectively. A higher exchange current, which means increase in the rate of electron transfer, was observed at the composite modified GCE. This increase in electron transfer (increase in reaction rate) can be attributed to the catalytic effect of the nanoparticles. The kinetics of $[Fe(CN)_6]^{3-/4-}$ increased by an order of magnitude at the PPyox/Ag-AuNPs/GCE//$[Fe(CN)_6]^{3-/4-}$ interface. It can thus be inferred that the PPyox/Ag-AuNPs/GCE catalyzed the redox reaction of $[Fe(CN)_6]^{3-/4-}$.

$Fe(CN)_6^{3-/4-}$ was also chosen as an electrochemical probe to investigate the prepared electrode because of their similar size and fast kinetics on glassy carbon electrodes, and confirm whether the alloy nanoparticles were deposited on the overoxidized polypyrrole. The response of $Fe(CN)_6^{3-/4-}$ is shown in Fig. 5. The CV curves at the PPyox/GCE (curve a) shows a redox peak with lower peak currents and larger peak to peak separations (ΔE_p = 143 mV) compared to that recorded with the bare GCE (Fig. 5, curve b, ΔE_p = 91 mV) an indicator that there was slower electron transfer. This can be attributed to the fact that overoxidized polypyrrole (PPyox) is prepared by oxidizing polypyrrole (PPy) to a higher oxidation state after which it becomes susceptible to nucleophilic attack [48] and results in the addition of carbonyl functionality to the pyrrolic rings with a consequent loss of conjugation and hence the loss of inherent electronic conductivity [48-49]. Moreover, the film is negatively charged with a large loss of electroactivity [50]. The negative charge of the layer should be unfavorable for the approaching of ferricyanide anions. After the Ag-AuNPs were assembled on the GCE (curve c), the peak current increased (54% increase) dramatically in comparison to that in curve b. The reason was that Ag-AuNPs with large specific surface area and good conductivity acted as conduction centers which facilitated the transfer of electrons, so much more $K_3Fe[CN]_6$ were accumulated on the modified electrode. However, the

purpose of over oxidizing the PPy was to exploit the fact that this process results in a polymer with pores on its surface, which creates a better condition for the attachment of nanoparticles. According to the cyclic voltammograms of the $K_3Fe(CN)_6^{3-/4-}$ redox probe shown in Fig. 5, after deposition of the Ag-Au alloy nanoparticles in the presence of electrodeposited PPyox-film on the GCE's surface (curve c), the peak current was enhanced by over 100% and the peak-to-peak separation (ΔE_p = 90) was reduced by 53 mV when compared to the CV recorded with PPyox film-modified electrode without the Ag-Au NPs. Relative to the bare GCE, the increased surface roughness and the newly induced surface functional groups and micro/nano catchment sites of the PPyox/GCE might have enhanced the loading of the nano-particles and, thus, created significant change in the surface area and the kinetics involved. This correlates well with the results shown in Fig. 4.

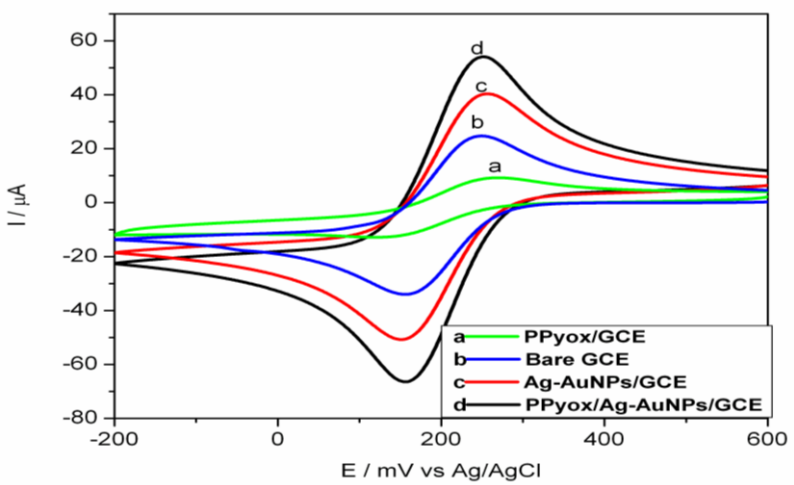

Figure 5. CVs recorded with PPyox/GCE (curve **a**), bare GCE (curve **b**), Ag-AuNPs/GCE (curve **c**) and PPyox/Ag-AuNPs/GCE (curve **d**) in the presence of $K_3Fe(CN)_6$ (5 mM) in aq. KCl (0.1 M). Scan rate: 50 mVs^{-1}.

3.3 Electrocatalytic Oxidation of AN and PHE

It was found that the PPyox/Ag-AuNPs/GCE had strong catalytic activity towards AN and PHE oxidation. Fig. 6 shows the CVs of 3.56 x 10^{-4} M AN in 1 M $LiClO_4$/acetonitrile at bare GCE (curve a), Ag-AuNPs/GCE (curve b), PPyox/GCE (curve c) and PPyox/Ag-AuNPs/GCE (curve d). As can be seen, the peak current at the Ag-AuNPs/GCE increased by about 30% compared to that of the bare GCE. This can be attributed to the catalytic effects of the nanoparticles. However, the contribution of modifying the GCE with PPyox (curve c) was most dominant as the PPyox/GCE alone exhibited about 70% increase in the anodic peak compared to the bare electrode. On deposition of the bimetallic Ag-Au nanoparticles onto the PPyox layer, the anodic peak showed a total increase by about 84% as shown by the response of the PPyox/Ag-AuNPs/GCE (curve d).

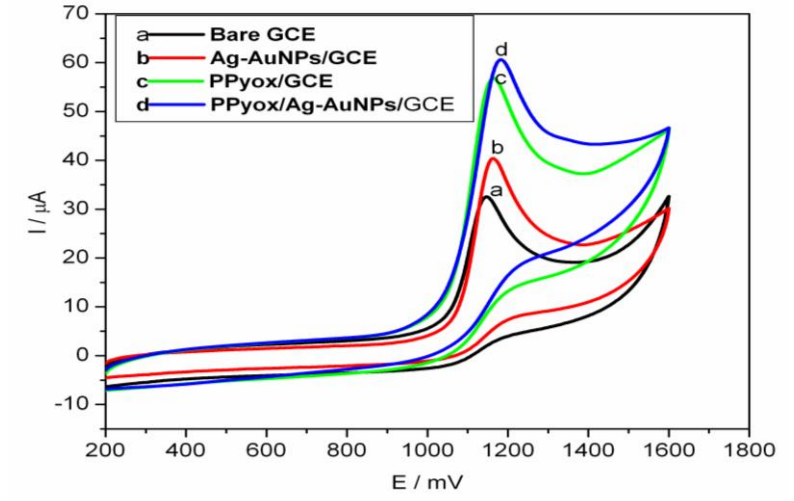

Figure 6. CV of 3.56 x 10^{-4} M anthracene at bare GCE (curve **a**), Ag-AuNPs/GCE (curve **b**), PPyox/GCE (curve **c**) and PPyox/Ag-AuNPs/GCE (curve **d**) in acetonitrile and 0.1 M $LiClO_4$ at a scan are of 50 mVs^{-1}.

Similar experiments were carried out for PHE, as shown in Fig. 7 (A). The Ag-AuNPs/GCE (curve b), PPyox/GCE (curve c), PPyox/Ag-AuNPs/GCE (curve d) exhibited peak currents which were about 32%, 37% and 51% higher than that of bare GCE (curve a), respectively. The largest increase in peak height was observed for PPyox/Ag-AuNPs/GCE an indicator that the composite had a strong electrocatalytic activity towards the oxidation of PHE. SWV experiments also indicated a similar trend (see Fig. 7 B). Therefore further studies were carried out only with the PPyox/Ag-AuNPs/GCE electrode.

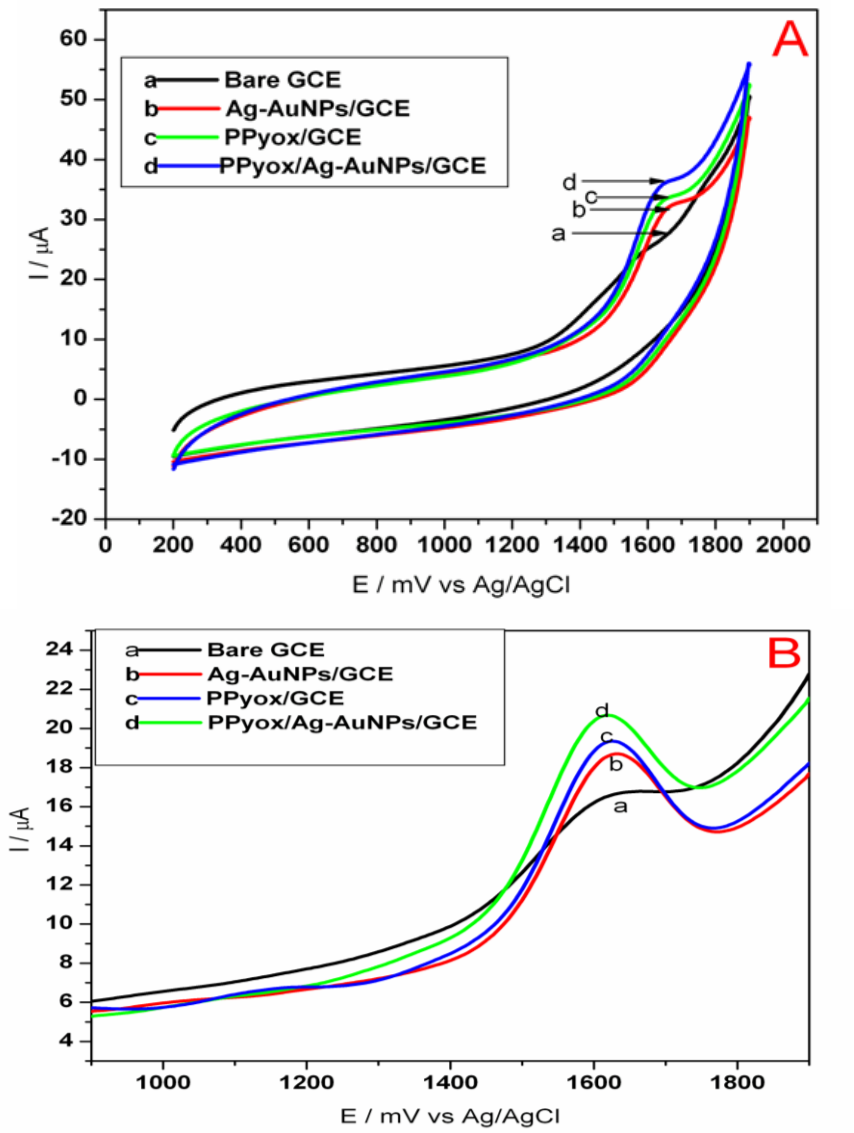

Figure 7. CVs **(A)** and SWVs (**B**) of 2.5 x 10^{-4} M PHE at bare GCE (curve **a**), Ag-AuNPs/GCE (curve **b**), PPyox/GCE (curve **c**) and PPyox/Ag-AuNPs/GCE (curve **d**) in acetonitrile and 0.1 M $LiClO_4$. The CV experiments were done at a scan rate of 50 mV s^{-1} while the SWV experiments, an amplitude of 25 mV, a frequency of 10 Hz and a step potential of 5 mV were applied.

3.4 Electrochemical Behaviour of PHE and AN on the Ppyox/Ag-AuNPs Modified Electrode

Fig. 8 shows cyclic voltammograms of AN (curve a), PHE (curve b) and blank (acetonitrile and 0.1M $LiClO_4$) (curve c) at a scan rate of 50 mV s^{-1} in acetonitrile and 0.1 M $LiClO_4$ when determined using PPyox/Ag-AuNPs/GCE. One oxidation peak was observed in both cases. The modified electrode showed no response (no electrochemistry) in absence of AN and PHE (curve c). Furthermore, the oxidation peaks for the oxidation of PHE and AN occurred at distinct potentials, 1.2 V and 1.6 V, respectively. Therefore the sensor can be useful for the simultaneous determination of the compounds in the same solution.

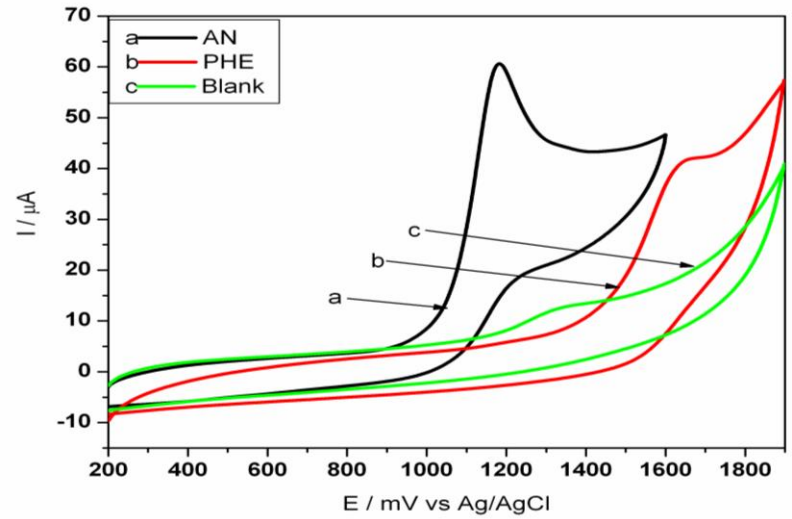

Figure 8. Voltammetric curves of 3.56 x 10^{-4} M solution of AN (curve **a**), 2.30 x 10^{-4} M solution of PHE (curve **b**) and 0.1 M $LiClO_4$ supporting electrolyte in acetonitrile (curve **c**) using PPyox/Ag-AuNPs/GCE. Scan rate: 50 mV s^{-1}.

To prove this, a mixture of PHE and AN (2.30 x 10^{-4} M each) were spiked into the electrolyte and acetonitrile. Two peaks were obtained corresponding to the oxidation of AN and PHE respectively as shown in Fig. 9 (peaks a and b). It was evident that the voltammogram peaks of the mixture solution of AN and PHE correlated well with that of their individual solutions (Fig. 8). It is noteworthy that, elimination of the fouling of the electrode surface by the oxidation products could be achieved and the precise determination of AN in the presence of PHE is possible at the PPyox/Ag-AuNPs/GCE. The voltammetric signals of AN and PHE remained unchanged in the subsequent potential sweeps, indicating that the PPyox/Ag-AuNPs modified electrode does not undergo surface fouling.

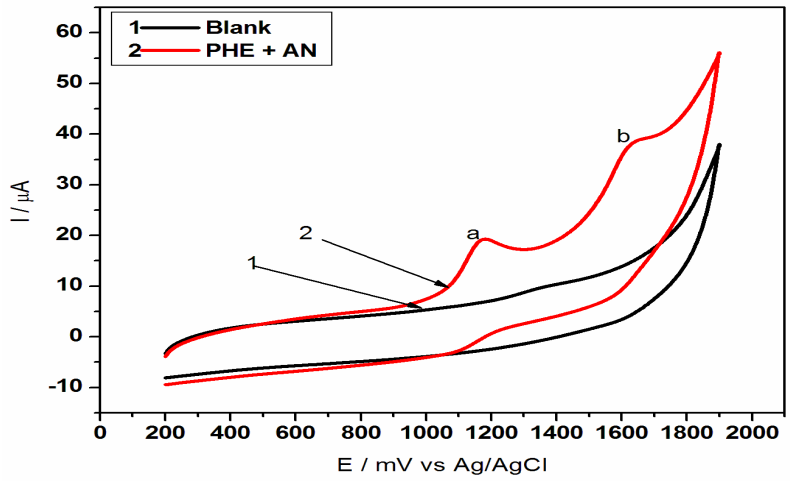

Fig. 9. CVs of PPyox/Ag-AuNPs/GCE in acetonitrile and 0.1 M $LiClO_4$ (blank) (**1**) and a mixture of AN and PHE (**2**). Scan rate: 50 mV s^{-1}.

3.5 Effect of Scan Rate on the Peak Current in the Binary Mixtures of AN and PHE

Fig. 10 (A) shows the cyclic voltammograms for the binary mixtures of 230 µM AN and 230 µM PHE in 0.1 M $LiClO_4$/acetonitrile at the PPyox/Ag-AuNPs modified electrode at different scan rates. The oxidation peak potentials of the two compounds were observed to shift positively with the increase in scan rate. In addition, the oxidation peak current for the oxidation of AN exhibited a linear relation to the square root of the scan rate, $v^{½}$, in the range from 20 to 450 mV s^{-1}, with the linear regression equation I_{pa}/A = -1.446 x 10^{-6} - 8.604 x 10^{-7} $v^{½}$ / $(mVs^{-1})^{½}$ (correlation coefficient, r^2 = 0.999), suggesting that the oxidation of AN at the modified electrode was diffusion-controlled process (Fig. 10 B). Simultaneously, the oxidation peak current for the oxidation of PHE also exhibited a linear relation to the square root of the scan rate, $v^{½}$, in the range from 20 to

450 mV s^{-1}, with the linear regression equation I_{pa}/A = -4.115 x 10^{-6} - 2.826 x 10^{-6} $\nu^{1/2}$ (mV $s^{-1})^{1/2}$ (correlation coefficient, r^2 = 0.999), suggesting that the oxidation of PHE at the modified electrode was also a diffusion-controlled process (Fig. 10 C).

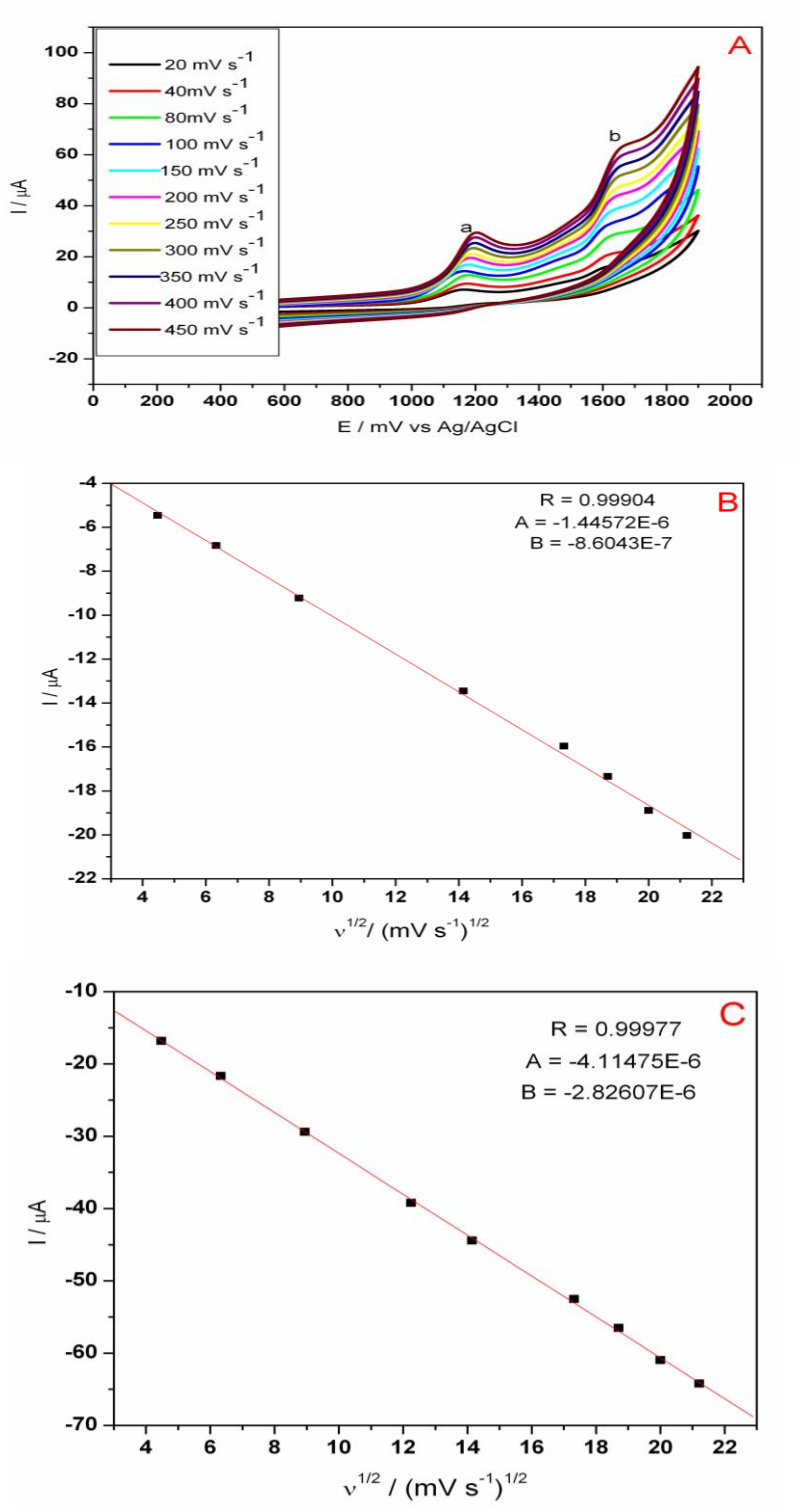

Figure 10. (A) CVs for the binary mixtures of 230 µM AN and 230 µM PHE in 0.1 M $LiClO_4$ and acetonitrile at the PPyox/Ag-AuNPs/GCE at different scan rates, (**B**) a plot of root scan rate versus peak current of AN and (**C**) PHE.

3.6 Simultaneous Determination of AN and PHE

A series of mixture standard solutions of AN and PHE, in which the concentration of one component was varied and the other was fixed were prepared and determined. Fig. 11(A) shows the SWV obtained when the concentration of PHE was kept constant and the concentration of AN was increased successively. The oxidative peak current for AN increased linearly with the increase in AN concentration in the range of 30 µM to 312 µM. The linear regression equation was I_{pa}/A = -9.268 x 10^{-7} + 2.736 x 10^{-8} C/µM (correlation coefficient, r^2 = 0.999) (see Fig. 11B) and the detection limit was 23.05 µM in the presence of 230 µM PHE. It can be observed that, with increasing concentration of AN, the current increased (Fig. 11 A, peak 1) while that of PHE (peak 2) kept almost constant. Thus it can be confirmed that the responses of AN and PHE at the modified electrode are independent.

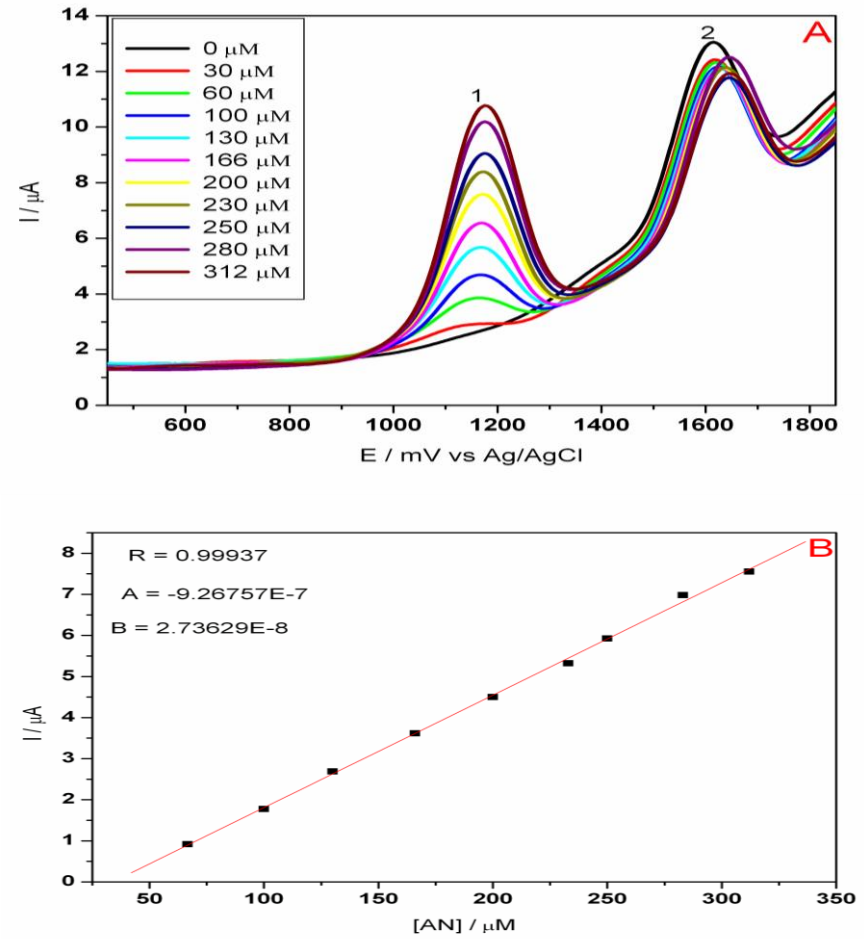

Figure 11. (A) SWV for the binary mixtures of AN and PHE at PPyox/Ag-Au NPs/GCE in 0.1 M $LiClO_4$/acetonitrile, [PHE] was kept constant and [AN] was increased and **(B)** a plot of concentration versus peak current of AN.

When the concentration of AN was kept constant and PHE concentration increased, there was a peak current increase with increase in concentration of PHE (Fig.. 12 (A) peak 2) while that of AN kept almost constant (Fig.. 12 (A) peak 1). The oxidative peak current increased linearly in the range of 30 µM to 280 µM. The linear regression equation was I_{pa}/A = -2.4 x 10^{-6} + 3.2 x 10^{-8} C / µM (correlation coefficient, r^2 = 0.999) (Fig.12 B) and the detection limit was 24.4 µM in the presence of 230 µM AN.

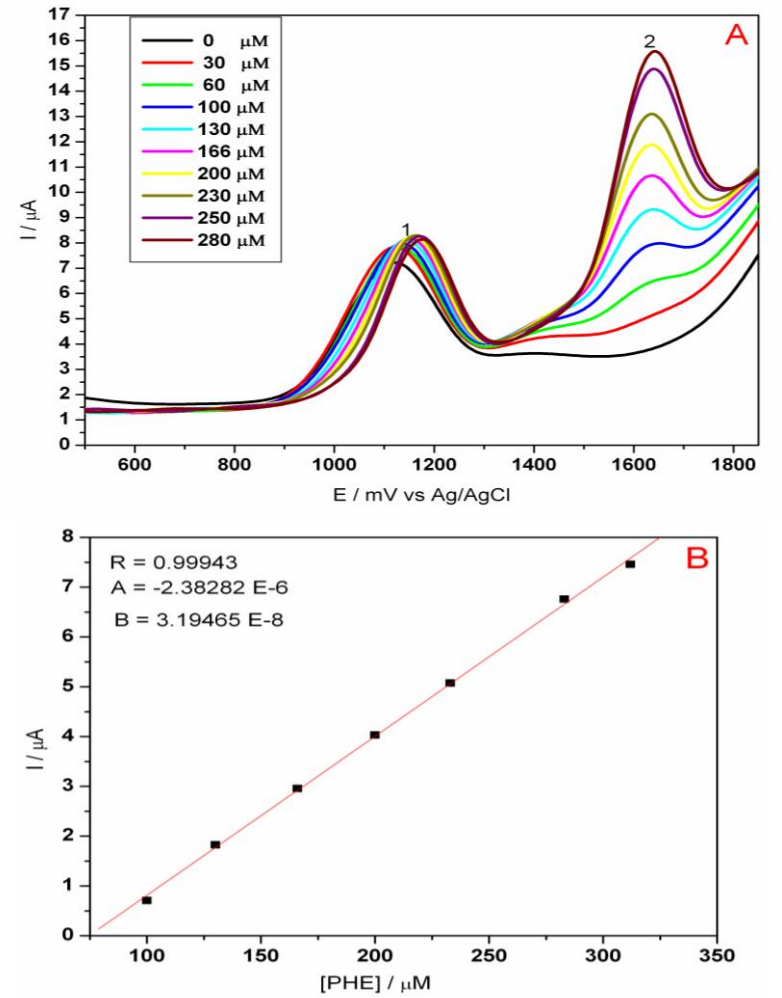

Figure 12. (A) SWV for the binary mixtures of AN and PHE at PPyox/Ag-Au NPs/GCE in 0.1 M $LiClO_4$/acetonitrile, [AN] was kept constant and [PHE] was increased and **(B).**a plot of peak current versus concentration of PHE.

Fig. 13 represents the SWV recordings at increasing concentrations of both AN and PHE. As can be seen, there was peak enhancement upon addition of both AN (Fig. 13 peak 1) and PHE solutions (Fig. 13 peak 2).

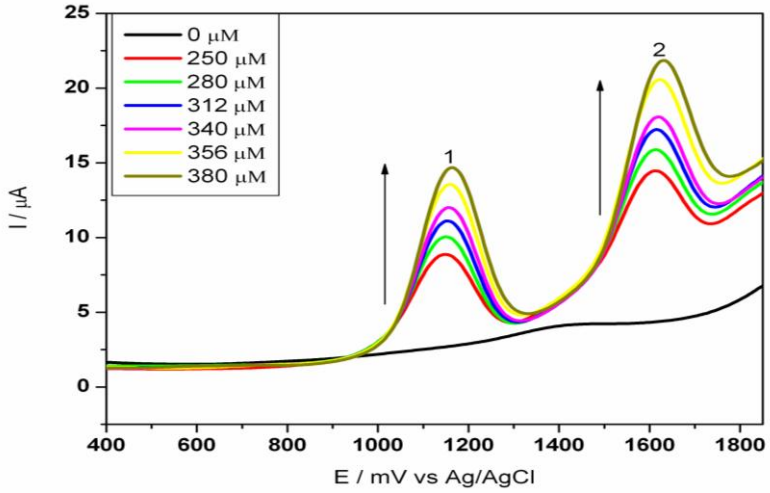

Figure 13. SWV for the binary mixtures of AN and PHE at PPyox/Ag-Au NPs/GCE in 0.1 M $LiClO_4$/acetonitrile, at increasing [AN] and [PHE]. (an amplitude of 25 mV, a frequency of 10 Hz and a step potential of 5 mV were applied).

It is worth noting that most of the analysis of PAHs using electrochemical methods involves the detection and determination of single PAHs [51-57]. However, the developed sensor was able to simultaneously detect AN and PHE in a mixture and that increasing the concentration of one does not affect the detection of the other. Thus, the responses of AN and PHE at the developed sensor are independent and that the sensor showed excellent sensitivity, selectivity and antifouling properties.

3.7 Reproducibility, stability and interference studies

Reproducibility and stability studies were performed by the analysis of three successive measurements (n = 3) of the SWV responses of the PPyox/Ag-Au/GCE sensor to 30 μM AN and PHE. A relative standard deviation of 1.5% was obtained indicating excellent reproducibility of the SWV measurements. The sensor response was also measured for a period of 3 weeks during which measurements were made at 4-day intervals in order to ascertain the storage stability of the sensor. The PPyox/Ag-Au/GCE sensor system was stored in the refrigerator at 4^{0} C in between measurements. During the 3 week storage period, the sensor retained 91% of the magnitude of its original signal. This can be attributed to the excellent stability of the film. Inorganic ions which are likely to be present in water samples especially water were investigated as possible sources of interferences. No interference could be observed for the following ions: Na^{+}, Cu^{2+}, Fe^{2+}, Mn^{2+}, Cl^{-}, SO_4^{2-} and NO_3^{-}.

IV. Conclusion

The present study demonstrated the fabrication of a novel electrochemical sensor based on a nano-porous PPyox template deposited Ag-Au alloy nanoparticles which formed a composite nano-electrode sensor, PPyox/Ag-Au/GCE. The PPyox/Ag-AuNPs/GCE exhibited a strong electrocatalytic activity towards the oxidation of AN and PHE. Moreover, the modified electrode was able to simultaneously detect AN and PHE. In SWV determination, the lower detection limits of AN and PHE were estimated to be about 23.05 μM and 24.4 μM, respectively. The catalytic activity of the PPyox film was significantly enhanced by the composition of Ag-Au alloy nanoparticles due to increasing electronic conductivity and effective surface area. The availability of the PPyox film and further design of its surface chemistry in combination with metal nanoparticles could be an interesting stratagem for the high efficient and high selective electrochemical sensor designs. The present sensor did not show the fouling effect usually caused by oxidation of anthracene and phenanthrene. Moreover, the developed sensor has good figure of merit in simultaneously analyzing more than one sample in the presence of multianalytes. It can thus be applied in the detection of anthracene and phenanthrene in water.

Acknowledgements

The authors appreciate the financial support from the Division of Research, Innovation and Linkages - Machakos University (Kenya) and the National Research Foundation (NRF) and Department of Science and Technology of the Republic of South Africa.

References

[1]. X Kang, Z Xiaoyong, C Peiang, M Jinyuan, A novel glucose biosensor based on immobilization of glucose oxidase in Chitosan on a glassy carbon electrode modified with gold-platinum alloy nanoparticles / multiwall carbon nanotubes, *Analytical Biochemistry, 369*, 2007, 71-79.

[2]. M Zhou, Z Shiyo, M Houyi, One-step synthesis of Au-Ag alloy nanoparticles by a convenient electrochemical method, *Physica E: Low-dimensional Systems and Nanostructures, 33 (1)*, 2006, 28-34.

[3]. S Devarajan, S Sampath, Phase transfer of Au–Ag alloy nanoparticles from aqueous medium to an organic solvent: effect of aging of surfactant on the formation of Ag-rich alloy compositions, *Journal of Colloid and Interface Science, 278*, 2004, 126–132.

[4]. T Masato, N Makoto, T Isao, Composition-activity relationships of carbon electrodes-supported bimetallic gold-silver nanoparticles in electrocatalytic oxidation of glucose, *Journal of electroanalytical Chemica, 615*, 2008, 51-61.

[5]. W Aiqin, C Yong-Fan, M Chung-Yuan, Au-Ag alloy nanoparticles as catalyst for CO oxidation : effect of Si/Al ratio of mesoporous suppor, *Journal of catalysts, 237*, 2006, 197-206.

[6]. R Xiangling, T Fangqiong, Preparation of Ag-Au nanoparticles and its application to glucose biosensor, *Sensors and actuators B, 110*, 2005, 358-363.

[7]. J Li, X Lin, Electrodeposition of gold nanoclusters on overoxidized polypyrrole film modified glassy carbon electrode and its application for the simultaneous determination of epinephrine and uric acid under coexistence of ascorbic acid, *Analytica Chimica Acta, 596(2)*, 2007, 222-230.

[8]. S Said, B Nancy, S Guillaume, The mechanism of pyrrole polymerization, *Royal society of Chemistry, 29*, 2000, 283-293.

[9]. T Abdulazeez, Polycyclic aromatic hydrocarbons, A review, *Environmental Science 3*, 2017, 1339841

[10]. I Juan, K Thomas, Simultaneous Determination of Polycyclic Aromatic Hydrocarbons, Alkylphenols, Phthalate Esters and Polychlorinated Biphenyls in Environmental Waters Based on Headspace–Solid Phase Microextraction Followed by Gas Chromatography–Tandem Mass Spectrometry, *Journal of Environmental Analytical Chemistry*, 4, 2017, 4

[11]. J Kielhorn, Guidelines for drinking water quality, Health criteria and other supporting information, world health organisation, Geneva, 2, 1998, 123-152.

[12]. M Marcia, B Denise, V Carine, Determination of Polycyclic Aromatic Hydrocarbons in Commercial Parenteral Formulations and Medications Using High-Performance Liquid Chromatography with Diode Array Detection, *Journal of AOAC International*, 100, 2017, 2

[13]. S Wilson, K Jones, Bioremediation of soil contaminated with polynuclear aromatic hydrocarbons (PAHs); a review, *Environmental Pollution, 81,* 1993, 229-249.
[14]. S Lundstedt, P Haglud, L Orberg Degradation and formation of polycyclic aromatic compounds during bioslurry treatment of an aged gasworks soil, *Journal of Environmental Toxicological Chemistry, 22*, 2003, 413.
[15]. S Shivender, K Abuzar, L Avasarala, K Ashok, G Kenneth, A Novel Protocol to Monitor Trace Levels of Selected Polycyclic Aromatic Hydrocarbons in Environmental Water Using Fabric Phase Sorptive Extraction Followed by High Performance Liquid Chromatography-Fluorescence Detection, *Separations, 4*, 2017, 22.
[16]. K Woodward, Determination of polyaroamatic hydrocarbon using immunoassays, *Science Total Environment 32*, 1984, 103.
[17]. Colmsjo A, The handbook of environmental chemistry part 1, PAHs and related coumpounds, *Springer-verlag, 3*, 1998, 55.
[18]. R Ferrer, J Guiteras, J Beltrán, Development of fast-scanning fluorescence spectra as a detection system for high-performance liquid chromatography Determination of polycyclic aromatic hydrocarbons in water samples *Journal of Chromatography A, 779 (1-2),* 1997, 123-130.
[19]. E Andrade, M López, L Muniategui, R Prada, F Fernández, Determination of polycyclic aromatic hydrocarbons (PAHs) in a complex mixture by second-derivative constant-energy synchronous spectrofluorimetry, *Talanta, 51,* 2000, 677-684.
[20]. J Szolar, Separation of PAHs by capillary electrophoresis (CE) equipped with laser-induced fluorescence, *Journal of molecular Resources 9*, 1996, 515.
[21]. Z Cai, Y Zhu, Y Zhang, Simultaneous determination of dissolved anthracene and pyrene in aqueous solution by synchronous fluorimetry, *Spectrochimica Acta Part A: Molecular and Biomolecular Spectroscopy, 69(1),* 2008, 130-133.
[22]. A Szekacs, D Knopp, R Niessner, A modified enzyme-linked immunosorbent assay (ELISA) for polyaromatic hydrocarbons, *Analytica chimica acta, 399*, 1999, 127-134.
[23]. K Li, R Chen, B Zhao, M Liu, A Karu, V Roberts, Q Li, Monoclonal Antibody-Based ELISAs for Part-per-Billion Determination of Polycyclic Aromatic Hydrocarbons: Effects of Haptens and Formats on Sensitivity and Specificity. *Analytical Chemistry, 71(2),* 1998, 302-309.
[24]. K Meisenecker, D Knopp, R Niessner, Development of an enzyme-linked immunosorbent assay (ELISA) for pyrene, *Analytical methods instrumentation 2(1)*: 1993, 14-118.
[25]. B Herikstad, A Haugen, H Hagen, Determination of polycyclic aromatic hydrocarbons in urine from coke-oven workers with a radioimmunoassay. *Carcinogenesis, 14(2),* 1993, 307-309.
[26]. N Kado, E Wei, Radioimmunoassay for benzo (a) pyrene, *Journal National Cancer Institute 61(1),* 1978, 221-225.
[27]. M Liu, Q Li, G Rechnitz, Flow injection immunosensing of polycyclic aromatic hydrocarbons; effect of haptens and formats on sensitivity and specificity. *Analytical Chemica,* 71, 1999, 302-309.
[28]. M Liu, G Rechnitz, Capacitive immunosensing of polycyclic aromatic hydrocarbons and protein conjuctes, *Analytical letters, 31(12),* 1998, 2025-2038.
[29]. T Vo-Dinh, G Griffin, K Ambrose, M Sepaniak, E Gardenhire, Antibody-Based Fiberoptics Biosensor for the Carcinogen Benzo(a)pyrene, *Applied Spectroscopy, 41,* 1987, 735-738.
[30]. K Fähnrich, M Pravda, G Guilbault Disposable amperometric immunosensor for the detection of polycyclic aromatic hydrocarbons (PAHs) using screen-printed electrodes, *Biosensors and Bioelectronics, 18 (1),* 2003, 73-82.
[31]. H Lee, D Cullen, B Kim, M Gu, Monitoring and classification of PAH toxicity using an immobilized bioluminescent bacteria, *Biosensensors and Bioelectronics, 18*, 2003, 571-577.
[32]. S Chang, Enhancement in the sensitivity of an immobilized cell-based soil biosensor for monitoring PAH toxicity, *Sensors and actuators B, 97*, 2004, 272-276.
[33]. P Pandey, H Weetall, Detection of aromatic compounds based on DNA intercalation using an evanescent wave biosensor, *Analytica Chimica, 67*, 1995, 787-792.
[34]. M Gu, Soil biosensor for the detection of PAH toxicity using an imobilized ecombinant bacterium and a biosurfactant, *Biosensors and Bioelectronics, 16*, 2001, 667-674.
[35]. D Ruey-an, L Shih-hui, Sol-gel-derived array DNA biosensor for detection of polycyclic aromatic hydrocarbons in water and biological samples, *Sensors and actuators B*, 2005, 323-330.
[36]. K White, An overview of immunotoxicology and carcinogenic polycyclic aromatic hydrocarbons, *Environment Carcinogenic Review C4*, 1986, 163-202.
[37]. K Rajeshwar, Environmental Electrochemistry Fundamentals and Applications in Pollution Abatement. *Academic Press, New York*, 1997.
[38]. S Mailu, W Tesfaye, P Ndangili, R Fanelwa, A Baleg, P Baker, E Iwuoha, Determination of Anthracene on Ag-Au Alloy Nanoparticles/Overoxidized-Polypyrrole Composite Modified Glassy Carbon Electrodes. Sensors, 10, 2010, 9449-9465.
[39]. A Pal, S Shah, V Kulkami, R Murthy, S Devi, Template free synthesis of silver-gold alloy nanoparticles and cellular uptake of gold nanoparticles in Chinese Hamster Ovary cell, *Materials Chemistry and Physics, 113(1),* 2009, 276-282.
[40]. S Yongsoon, A Bruce, E Gregory Facile stabilization of Gold-Silver alloy nanoparticles on cellulose nanocrystal, *Journal of Physical Chemistry C, 112*, 2008. 4844-4848.
[41]. J Fang, C Zhong, R Mu, The study of deposited silver particulate films by simple method for efficient SERS, *Chemical Physics Letters, 401, (1-3),* 2005, 271-275.
[42]. A McFarland, C Mirkin, R Van, H Godwin, Synthesis of gold nanoparticles, *Journal of Chemical Education, 81,* 2004, 544.
[43]. J Zhu, Theoretical study of the optical absorption properties of Au-Ag bimetallic nanospheres, *Physica E: Low-dimensional Systems and Nanostructures, 27(1-2),* 2005, 296-301.
[44]. P Angshuman, S Sunil, D Surekha, Preparation of Silver–Gold Alloy Nanoparticles at Higher Concentration Using Sodium Dodecyl Sulfate, *Journal of Chemistry, 61,* 2008, 66.
[45]. S Link, M El-Sayed, Alloy Formation of Gold−Silver Nanoparticles and the Dependence of the Plasmon Absorption on Their Composition, *Journal of Physical Chemistry B, 103(18),* 1999, 3529–3533.
[46]. B Speiser, M Stratman, Unwin P.R. (Eds.), Encyclopedia of Electrochemistry. WILEY-VCH Verlag GmgH and CO. kGaA,Weinheim chapter 2, 2003.
[47]. PM Monk, Fundamentals of Electroanalytical Chemistry. Newyork, USA: John Wiley & Sons, 2001, 264-266.
[48]. F Beck, M Oberst, B Bunsenges, Organic electrochemistry in the solid state-overoxidation of polypyrole, *Journal of Physical Chemistry, 91(9),* 1987, 967-974.
[49]. P Christensen, A Hamnett, In situ spectroscopic investigations of the growth, electrochemical cycling and overoxidation of polypyrrole in aqueous solution. *Electrochimica Acta, 36(8),* 1991, 1263-1286.
[50]. D Van, C Martin, Fibrillar electronically conductive polymers show enhanced rates of charge transport, *Synthetic Metals, 36(2),* 1990, 275-281.

[51]. P Abra, G Blaženka, S Draženka, N Andrew, In situ electrochemical method for detecting freely dissolved polycyclic aromatic hydrocarbons in water, *Environmental Chemistry, 11*, 2014, 173–180.
[52]. R Hlamulo, T Oluwakemi, E Christopher, W Tesfaye, I Emmanuel , Electrochemical Interrogation of G3-Poly(propylene thiophenoimine) Dendritic Star Polymer in Phenanthrene Sensing, *Sensors, 15*, 2015, 22343-22363.
[53]. W Maochao, D Shuo, L Shan, Z Xiangli, X Fangquan, Z Changli Electrochemical determination of Phenanthrene based on anthraquinone sulfonate and poly diallyldimethylammonium chloride modified indium–tin oxide electrode, *RSC Advances 5*,2015, 48811.
[54]. T Oluwakemi, J Nazeem, E Christopher, P Keagan, F Rachel, R Hlamulo, M Kerileng, V Suru, G Priscilla, I Emmanuel, Electro-oxidation of anthracene on polyanilino-graphene composite electrode, *Sensors and Actuators B, 205*, 2014, 184–192.
[55]. E Omolola, S Abolanle, E Eno, Electrochemical Detection of Phenanthrene Using Nickel Oxide Doped PANI Nanofiber Based Modified Electrodes, *Journal of Nanomaterials*, 2016, 1-12.
[56]. L Usman, P Liu, L Franz, Conductometric Sensor for PAH Detection with Molecularly Imprinted Polymer as Recognition Layer, *Sensors 18*, 2018, 767.
[57]. Z Yan, D Pingge, Z Huisheng, Detection of Anthracene in Real Water Samples with a Label-free Amperometric Immunosensor, *Advanced Materials Research, 185*, 2011, 547-551.

IOSR Journal of Applied Chemistry (IOSR-JAC) is UGC approved Journal with Sl. No. 4031, Journal no. 44190.

Stephen Nzioki Mailu . " Simultaneous Detection of Anthracene and Phenanthrene on Ag-Au alloy nanoparticles/overoxidized-polypyrrole Composite Modified Carbon Electrode." IOSR Journal of Applied Chemistry (IOSR-JAC) 12.2 (2019): 65-80.